Int J Earth Sci (Geol Rundsch) (2006) 95: 491–503
DOI 10.1007/s00531-005-0038-6

ORIGINAL PAPER

Ph. Münch · J.-J. Cornée · G. Féraud
J.-P. Saint Martin · M. Ferrandini · F. Garcia
G. Conesa · S. Roger · M. Moullade

Precise $^{40}Ar/^{39}Ar$ dating of volcanic tuffs within the upper Messinian sequences in the Melilla carbonate complex (NE Morocco): implications for the Messinian Salinity Crisis

Received: 19 April 2004 / Accepted: 10 July 2005 / Published online: 23 September 2005

Abstract The Melilla carbonate complex (NE Morocco) is the only area of the Paleo-Mediterranean Sea where volcanic activity was present throughout most of the Messinian. $^{40}Ar/^{39}Ar$ dating of volcanic tuffs interbedded within the upper Messinian sedimentary deposits, known as the Terminal Carbonate Complex (TCC), yields accurate ages of paleoenvironmental and sea-level changes related to the Messinian Salinity Crisis. The new chronologic data (1) provide an average of 5.95–5.99 Ma for the base of the TCC, thus being synchronous with the onset of the Messinian Salinity Crisis, (2) demonstrate for the first time that the basal unconformity of the TCC does not represent a hiatus of long duration, (3) define a precise time line at 5.87 ± 0.02 Ma (2σ) corresponding to sedimentary rocks exhibiting a lateral transition between continental and marine deposits typical of the TCC and (4) yield evidence that emersion of the Melilla platform during deposition of the TCC is partly related to tectono-magmatic activity. An erosional surface, capping the TCC deposits in the Melilla basin, is related to the major Messinian Mediterranean drawdown. The duration of the hiatus, associated with this surface, is estimated to be at most 450 kyr, but is probably shorter.

Keywords Melilla · $^{40}Ar/^{39}Ar$ · Messinian · Terminal carbonate complex · Salinity crisis

P. H. Münch (✉) · J.-P. S. Martin · F. Garcia · G. Conesa
S. Roger · M. Moullade
UMR 6019-DRPC, Université de Provence, case 67, 3 pl.,
V. Hugo, 13331 Marseille Cedex 3, France
E-mail: philippe.munch@up.univ-mrs.fr
Tel.: +33-4-91106343
Fax: +33-4-91106342

J.-J. Cornée
UMR 5125-PEPS, Bât. Géode, 11-43 Bd du 11 novembre,
Université Claude Bernard Lyon I,
69622 Villeurbanne Cedex, France

G. Féraud · M. Moullade
UMR 6526 Géosciences Azur, CNRS-UNSA,
06108 Nice Cedex 02, France

M. Ferrandini
Laboratory de Géologie, Université de Corse,
BP 52, 20250 Corte, France

Introduction

The famous Messinian Salinity Crisis (MSC; Hsü et al. 1977) occurred during the Late Miocene in the Paleo-Mediterranean Sea and is mainly represented by thick and regionally extensive evaporitic deposits in Sicily and the Central Mediterranean region which are classically divided into two main units: Lower and Upper Evaporites. The evaporites are related to a catastrophic sea-level drawdown and include brackish-to-freshwater "Lago-mare" deposits. Events linked to the MSC have been dated principally within outcrops of the Paleo-Mediterranean using magnetostratigraphy or astrochronology, or both in the "deep" basinal sequences (Gautier et al. 1994; Krijgsman et al. 1999, 2001).

Shallow-water carbonate complexes associated with the MSC and located along the margins of the Paleo-Mediterranean Sea have undergone a significant amount of research because these deposits contain a high-resolution record of paleoenvironmental and sea-level changes. A general description of the carbonate complexes from bottom to top includes: (1) retrogradational deposits (marls, conglomerates, bioclastic limestones); (2) a prograding bioclastic and younger reefal platform ("fringing reefs" or "reef complex"); (3) mixed siliciclastic-oolitic coastal deposits, including large microbial build-ups, known throughout the Western Mediterranean as the "Terminal Carbonate Complex" (TCC) bounded by two major unconformities (*sensu* Esteban 1979); (4) brackish-to-freshwater continental deposits (Lago-Mare-like facies). Correlations between basinal and coastal sequences are fundamental in understanding the MSC; however, they have been highly debated

because of the lack of precise chronological constraints within the carbonate complexes (Krijgsman et al. 2001; Riding et al. 1998, 1999, 2000; Fortuin et al. 2000; Montgomery et al. 2001; Rouchy et al. 2003). Limited chronological constraints within these Messinian shallow-water carbonates are related to (1) the lack of age-diagnostic planktic foraminifera; (2) numerous difficulties in interpreting magnetostratigraphic data (problems include low natural remanent magnetization, discontinuous sedimentation and diagenetic overprints); (3) inadequate data to produce decisive astrochronology and (4) the scarcity of intercalations of datable volcanic layers.

The timing of the deposition of MSC evaporites and the main MSC sea-level drawdown have been highly debated, highlighting the importance of why precise dating of TCC deposits remains crucial to better understand the MSC:

1. Evaporite deposition within basins at the margins of the Paleo-Mediterranean Sea, which corresponds to the MSC onset, has been correlated to the Geomagnetic Polarity Time Scale (GPTS) and the Astrochronological Polarity Time Scale (APTS) yielding an age of about 5.94–5.96 Ma (Gautier et al. 1994; Krijgsman et al. 1999, 2001). These evaporites have been correlated differently within the stratigraphic succession of Messinian sedimentary deposits. Some authors correlated them with an erosional surface at the boundary separating prograding reefs and TCC, assuming that these evaporites are the Lower Evaporites of Sicily and Central Mediterranean and were deposited during a low-stand system tract (Rouchy and Saint-Martin 1992; Cunningham et al. 1994, 1997; Roep et al. 1998). Others assumed that they are the Upper Evaporites and were deposited during a transgression following a 400 kyr hiatus represented by the same surface that separates the prograding reefs from the TCC (Riding et al. 1998, 1999). More recently it has also been proposed, but not yet demonstrated, that they correspond to the Lower Evaporites and are equivalent to the TCC (Cornée et al. 2002, 2004; Fortuin and Krijgsman 2002).
2. It has been proposed that the main drawdown of the Paleo-Mediterranean Sea during the MSC occurred either before deposition of the Lower Evaporites within marginal basins (Riding et al. 1999; Rouchy and Saint-Martin 1992) or after their deposition (Krijgsman et al. 1999, 2001; Clauzon et al. 1996). This drawdown is correlated, within the carbonate complexes, to a major erosional surface located either at the contact between the prograding reefs and the TCC (Rouchy and Saint-Martin 1992; Martin and Braga 1994; Braga and Martin 1996; Cunningham et al. 1997; Riding et al. 1999) or above the TCC (Clauzon et al. 1996; Roep et al. 1998; Krijgsman et al. 2001; Fortuin and Krijgsman 2002).

The Melilla carbonate complex, NE Morocco (Fig. 1), is one of the more complete Messinian stratigraphic successions and is known for the occurrence of numerous datable K-rich volcanic layers (Cunningham et al. 1994, 1997; Roger et al. 2000; Münch et al. 2001; Cornée et al. 2002; Kuiper 2003). Nevertheless, chronological data from the TCC are still too scarce and imprecise to accurately define relations between the platform sequences and the main events of the MSC. Moreover, it has been recently proposed that the uppermost Messinian sediments of the Melilla basin could correspond to Lago-Mare-like deposits, indicative of an early (~5.8 Ma) dilution of the Melilla basin by freshwater (Rouchy et al. 2003). The purpose of this study is to establish an updated and precise geochronological framework for the TCC of Melilla basin by extending the existing $^{40}Ar/^{39}Ar$ dataset (Cunningham et al. 1994, 1997; Roger et al. 2000; Münch et al. 2001;

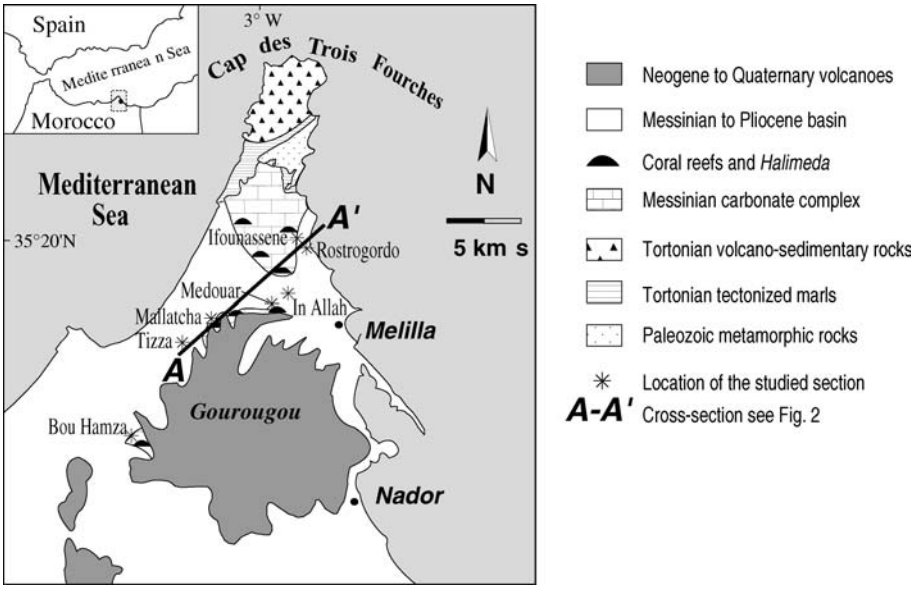

Fig. 1 Simplified geological map of the study area near Melilla and Nador with locations of the studied sections

Cornée et al. 2002; Kuiper 2003) to key stratigraphic levels. Our new chronological data combined with recent sedimentological and biostratigraphical investigations at the basin scale provide new constraints for the timing and the evolution of the MSC.

Geological setting and studied sections

The Melilla carbonate complex is mainly located on the northern margin of a post-nappe basin in the Rif region (Fig. 1; Guillemin and Houzay 1982). It is represented by a bioclastic, reefal and oolitic platform, which has been extensively studied (e.g. Guillemin and Houzay 1982; Cunningham et al. 1994, 1997; Saint Martin et al. 1991; Cornée et al. 1996; Roger et al. 2000; Münch et al. 2001; Cornée et al. 2002; Cunningham and Collins 2002; Garcia et al. 2004). In this study, we will use the most recent stratigraphic and sedimentological framework (e.g. Cornée et al. 2002, 2004), which differs from the one previously established by Cunningham et al. (1994, 1997). The differences between these two frameworks have already been extensively discussed in Saint Martin and Cornée (1996), Cornée et al. (1996, 2002, 2004), Roger et al. (2000), Münch et al. (2001, 2003) and Garcia et al. (2004). Three main cycles (Fig. 2) can be defined within the stratigraphic succession (Cornée et al. 2004): (1) a first cycle (cycle 1), Tortonian (?) to Messinian in age, is composed of retrogradational conglomerates overlain by a bioclastic ramp, a progradational bioclastic unit and a younger reefal platform, merging laterally into marls and alternating marls and diatomites towards the basin (the two or three youngest prograding reefs are associated with *Halimeda*-rich slopes extending far basinward and constituting an index-bed) ; (2) a second cycle (cycle 2), Messinian in age, characterized by a very flat aggrading–retrograding geometry (Cornée et al. 2002, 2004) and, from bottom to top, by reefs, giant microbial buildups and mixed siliciclastic-oolitic deposits with associated stromatolites; and (3) a third cycle (cycle 3), possibly Pliocene in age (Guillemin and Houzay 1982; Rouchy et al. 2003), that mainly developed in the southwestern part of the basin, and is composed of silty to sandy marls and littoral shallow marine *Isognomon*-rich beds.

Cycle 2 corresponds to the TCC (*sensu* Esteban 1979) based on its lithology and unconformities that bound it at the top and bottom. Seven sections, from the northern

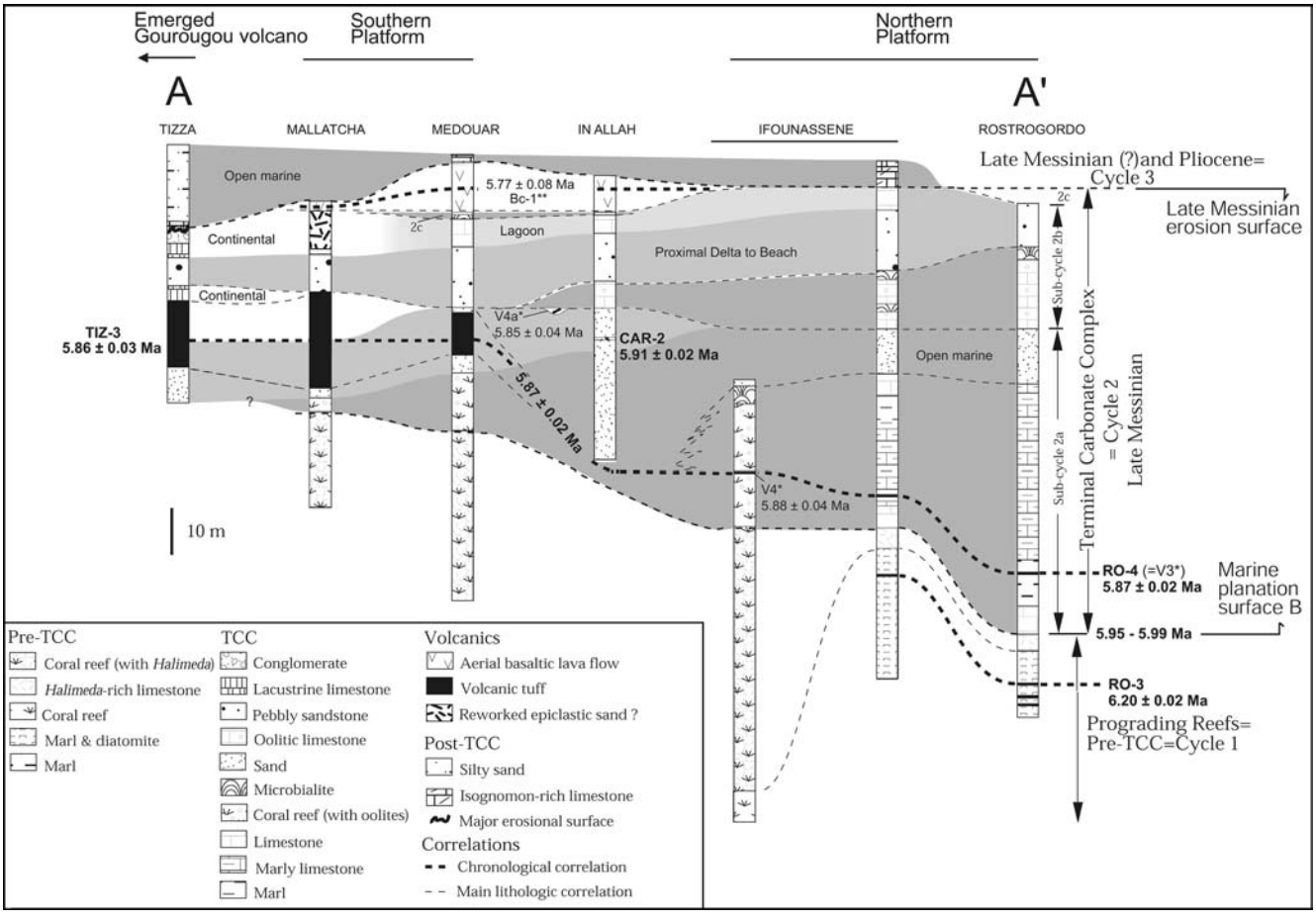

Fig. 2 Correlation of the studied Messinian TCC sections and depositionnal environments (*grey scale*). The sections have been arranged in order to have the base of the basaltic lava flow lying flat. Previous geochronological data: *Cunningham et al. (1994, 1997); **Cornée et al. (2002)

platform edge to the foothill of the Gourougou volcano (Fig. 2), were studied. The lower unconformity, which is positioned between cycles 1 and 2 (surface B in Cornée et al. 2004) is considered as a marine planation surface associated with a minor drop in sea level (Cornée et al. 2002). From the reef-talus slopes (Ifounassene section) to the proximal basin (Rostrogordo section), two volcanic tuffs have been found surrounding the *Halimeda* index-bed (Fig. 2). The tuffs from the Rostrogordo section (Ro-3 and Ro-4, 7.3 m below and 5.5 m above the *Halimeda* index-beds, respectively) are precisely dated ($^{40}Ar/^{39}Ar$ ages), which allows us to propose an age for the base of the TCC and an estimate of the possible time gap associated with the basal unconformity of the TCC. Within the TCC, two major sub-cycles have been recognized, representing two main transgressive–regressive trends (Garcia et al. 2004). A third sub-cycle (sub-cycle 2c) can be distinguished but it is very thin, incomplete and mainly exposed in the area around Medouar and In Allah (Fig. 2; Garcia et al. 2004). The oldest sub-cycle (sub-cycle 2a, Fig. 2) corresponds to the termination of the construction of the Melilla reef complex and overlying siliciclastic deposits, and the younger (sub-cycle 2b, Fig. 2) corresponds to the development of a mixed oolitic shallow ramp during the progressive infill of the Melilla basin. The sub-cycle 2a leads to an approximately flat topography of the coastal zone floor under very shallow marine environments, with some very localized and temporary emersions. One volcanic tuff (Tiz-3) and one tuffaceous sand layer (Car-2), both occurring within the deposits of the sub-cycle 2a (Fig. 2), were also sampled for $^{40}Ar/^{39}Ar$ dating. The volcanic tuff (sample Tiz-3) is located a few metres above the last reef in the Mallatcha and Medouar sections (Fig. 2). From its geographic extension and the typical pinkish colour, the volcanic tuff (sample Tiz-3) constitutes an index-bed marker within this region known as the "Pink Tuff" (Azdimoussa and Bourgois 1993; El Bakkali et al. 1998). The sample Car-2 is intercalated within shoreface sandy facies 5 m below the top of the sub-cycle 2a deposits, and 20 cm below a localized paleosoil (Fig. 2). The sub-cycle 2b exhibits increasing continental influences. However, brackish to marine environments persist until the end of TCC deposition as oolitic facies or stromatolites, or both, are reported in the sub-cycle 2c deposits in the Medouar and In Allah sections (Garcia et al. 2004). Near the top of the TCC deposits there is a sub-aerial lava flow dated at 5.77 ± 0.08 Ma (Cornée et al. 2002) or an erosional surface, both observable in the southwestern parts of the Melilla basin and both indicative of an emersion of regional extent (Guillemin and Houzay 1982; Cornée et al. 2004). Within the northern platform and basinal areas, the erosional surface is poorly identified as the cycle 3 deposits conformably rest upon the top of cycle 2 and the aerial lava flow is lacking.

The lower part of cycle 3 is represented by silty marls that are only preserved in the bottom of the deepest incised valley (Guillemin and Houzay 1982). Overlying the marls are yellow sands and, towards the shore, the *Isognomon* index-beds (Cornée et al. 1996). As no volcanic layer is present within cycle 3, it was previously assigned to the Pliocene on the basis of the sporadic presence, within the upper yellow sands, of *G. margaritae margaritae* and *Sphaeroidinellopsis* spp. (Guillemin and Houzay 1982) and the occurrence of *Ceratolithus acutus* (Rouchy et al. 2003). As the lowermost marls are azoic, a definite age for the onset of the marine flooding during early deposition of cycle 3 is uncertain, and could vary from Late Messinian to Early Pliocene (Cornée et al. in preparation).

$^{40}Ar/^{39}Ar$ dating

Description of volcanic layers

Samples Ro-3 and Ro-4, from the Rostrogordo section (Fig. 2), are non-welded sea-rafted pumice horizons that contain some rare bioclasts. They were deposited in a very low-energy environment as indicated by the surrounding muddy sediments. The mineralogical composition of both tuffs is dominated by sanidine, plagioclase and biotite which are associated with clinopyroxene only in sample Ro-3. The crystals are euhedral and always included in the pumice clasts. These pumice horizons may probably correspond to two large pyroclastic eruptions.

Sample Tiz-3 is a non-welded pumiceous tuff with a typical pinkish colour. It corresponds to a thick volcanic breccia from which the clasts are predominantly rhyolitic and trachytic pumices, and volcanic lithic fragments. The rhyolitic and trachytic pumices are located in the upper and lower portion of the pyroclastic flow probably representing the inverted sequence of magma erupted from a zoned chamber. The trachytic pumices are porphyritic and their mineralogy is dominated by sanidine associated with biotite, plagioclase and minor oxides. The rhyolitic pumices are sub-aphyric with sanidine and plagioclase microphenocrysts. The maximum thickness (≈20 m) of the whole tuff is located at the foothill of Gourougou volcano (Tizza and Mallatcha sections) and decreases markedly to the north in the study area (Fig. 2). It also shows a rapid decrease in the number of clasts and their size with distance from the source. It is likely that it was produced by pyroclastic flows; however, epiclastic processes cannot be ruled out, especially with increasing distance from the source. All sanidine crystals selected for dating were separated from trachytic pumice blocks (size > 15 cm) sampled near the Gourougou volcano zone (Tizza section; Fig. 2), in order to limit the potential of contamination from accidental ejecta and post-eruption epiclastic reworking processes.

Sample Car-2 is a tuffaceous sandstone (*sensu* Cas and Wright 1988) containing mainly crystal fragments and pumice clasts (size < 1 cm). It is a few centimetres thick, exhibits normal grading and occurs as a discontinuous

layer infilling an irregular paleotopography between small-scale dunes. The base of the tuffaceous sandstone is mainly composed of small-sized broken crystals while larger pumice clasts are present above. The principal mineral constituents are sanidine and plagioclase. Because of the high energy of the depositional environment, epiclastic reworking and redeposition are highly suspected whereas pyroclastic falls cannot be completely ruled out.

Methodology

$^{40}Ar/^{39}Ar$ analyses were performed on single sanidine crystals. Samples were crushed and the sanidines were separated using conventional techniques (magnetic separator, heavy liquids) and semi-quantitative chemical analysis under a XL-30 Philips Environmental Scanning Electron Microscope (ESEM) equipped with an energy dispersive spectrometer (EDAX DX4). All the crystals were ultrasonically cleaned in baths of pure acetone, alcohol and distilled water in order to remove alteration products and glass. Finally, sanidine crystals, ranging from 0.2 to 1.4 mm in size, were hand-picked under a binocular microscope. In order to confirm that all analyzed grains are sanidine, ESEM analyses were used to produce a rough composition of each grain selected for dating. This technique was tested and described in more detail in Roger et al. (2000).

The selected samples were irradiated for 5 h in the McMaster University reactor (ON, Canada) in position 5c. The Fish Canyon Tuff Sanidine was utilized as a monitor (FCTs, 28.02 Ma; Renne et al. 1998). Seven clusters of five grains of sanidine monitor were included in a 30-mm-long irradiation can, and the distances between them were lower than 7 mm. No flux gradient could be detected along the irradiated can, and we estimated an error of about ± 0.2% on the $^{40}Ar_{rad}/^{39}Ar_K$ measured on the monitor. The total neutron flux density during irradiation was 1.3×10^{18} n/cm^2 .

Sanidine crystals were step heated or fused or both using a SYNRAD CO_2 continuous laser with a maximum output power of 50 W. Isotopic analyses were carried out on a VG 3600 mass spectrometer working with a Daly detector system. Typical blank values of the full extraction and purification system, routinely measured every three steps, were in the range of $3–6\times10^{-13}$, $3–25\times10^{-14}$ and $1–2\times10^{-14}$ ccSTP at masses 40, 39 and 36, respectively. Beam intensities of Ar isotopes were typically in the order of 500–2,500 and 2,000–25,000 times the blank level, in total fusion experiments, and in the order of 30–2,500 and 100–7,000 times the blank values in the fused step during step heating experiments, for the ^{40}Ar and ^{39}Ar, respectively. The value for ^{36}Ar was indistinguishable from the blank value in some cases. Mass discrimination was monitored by analyzing Ar from a well-known air pipette volume, and the $^{40}Ar/^{36}Ar$ ratio was measured with a maximum error of ±0.5% (1σ).

The results are reported on age spectra of Fig. 3. Plateau ages are defined at least by three successive steps showing consistency within a 2σ confidence interval and carrying at least 70% of the ^{39}Ar released. For the two samples dating the base of TCC (Ro-3 and Ro-4), direct fusion experiments were also conducted to evaluate the homogeneity of the grain population in order to detect xenocrysts or post-volcanic reworking processes or both. For single fusion experiments, a pre-degassing step was always performed before fusion to reduce eventual contamination from alteration phases. The fuse steps correspond to more than 97% of the total ^{39}Ar released. All errors on the plateau ages, single fusion ages, isochron ages and weighted mean ages are quoted at a 2σ confidence level and do not include the errors associated with the age of the monitor. The value of the error for the $^{40}Ar^*/^{39}Ar_K$ ratio of the monitor is included on error calculation for plateau ages and single fusion ages. The full $^{40}Ar/^{39}Ar$ data set is shown in Table 1.

Results

Four single crystals from the Ro-3 tuff (Fig. 2) were step heated. Their displayed plateau ages (including three concordant ages) range from 6.15 ± 0.03 to 6.25 ± 0.02 Ma and correspond to at least 80% of the ^{39}Ar released (Fig. 3a, b). Seven total fusion analyses performed on single crystals yielded similar ages ranging from 6.16 ± 0.03 to 6.27 ± 0.02 Ma. The homogeneous $^{37}Ar_{Ca}/^{39}Ar_K$ ratio (Fig. 3a, b) of steps defining a plateau demonstrates the purity of the analyzed sanidine grains. The age distribution of all data (plateau and single fusion ages) gives a peak value of 6.20 Ma corresponding to the weighted mean age (Fig. 4). The weighted mean age of seven concordant ages (two plateau ages and five single fusion ages, plain symbols in Fig. 4) is 6.20 ± 0.02 Ma and corresponds to the accepted age for this sample. The inverse isochron diagram ($^{36}Ar/^{40}Ar$ vs. $^{39}Ar/^{40}Ar$) for all data (not given) produces an age of 6.20 ± 0.03 Ma (MSWD = 2.3 and initial $^{40}Ar/^{36}Ar$ ratio of 434 ± 51). When we recalculate an age from the plateau fractions and fused steps only, the value is 6.15 ± 0.05 Ma (MSWD = 2.6 and initial $^{40}Ar/^{36}Ar$ ratio of 1969 ± 1037). These $^{40}Ar/^{36}Ar$ ratios are far from the accepted atmospheric value (295.5); this is a consequence of the clustering of high-precision data on the diagram, resulting from low atmospheric contamination.

Among the five step-heated single sanidine crystals from the Ro-4 tuff (Fig. 2), four of them yielded concordant plateau ages ranging from 5.84 ± 0.04 to 5.89 ± 0.04 Ma, corresponding to more than 93% of the ^{39}Ar released (Fig. 3c, d). One plateau age at 5.77 ± 0.04 Ma (Ro-4b) is slightly younger. Here also the $^{37}Ar_{Ca}/^{39}Ar_K$ ratios show that the gas released from heating steps defines a plateau corresponding to pure and homogeneous sanidine (Fig. 3c, d). The weighted mean age calculated from the four concordant plateau

Table 1 Full $^{40}Ar/^{39}Ar$ dataset. Step = step number (laser probe)

Sample	J	Step	% ^{40}Ar atm.	39Ar (%)	$^{37}Ar_{Ca}/^{39}Ar_K$	$^{40}Ar^*/^{39}Ar_K$	Apparent age (Ma)		Plateau Age (Ma) ± 2σ	Accepted Age (Ma) ± 2σ
Ro-3a	0.002520	1	35.96	0.1	0.023	1.945	8.80	± 2.84		
		2	13.90	0.4	0.034	1.305	5.91	± 0.63		
		3	5.55	0.7	0.021	1.323	5.99	± 0.29		
		4	0.00	1.6	0.021	1.383	6.26	± 0.17		
		5	0.83	2.8	0.020	1.365	6.18	± 0.10		
		6	0.16	11.3	0.018	1.370	6.20	± 0.03		
		7	0.00	17.8	0.018	1.374	6.22	± 0.02		
		8	0.34	10.4	0.017	1.369	6.20	± 0.02	6.22 ± 0.02	
		9	1.02	8.1	0.018	1.361	6.16	± 0.03		
		fuse	0.00	46.7	0.017	1.379	6.24	± 0.01		
						Integrated age =	*6.22*	*± 0.01*		
Ro-3b	0.002520	1	56.64	0.1	0.051	0.985	4.46	± 3.29		
		2	9.83	0.5	0.031	1.360	6.16	± 0.74		
		3	7.16	0.9	0.024	1.297	5.87	± 0.36		
		4	3.71	1.7	0.019	1.334	6.04	± 0.26		
		5	2.09	5.9	0.018	1.348	6.10	± 0.07		
		6	1.22	11.1	0.018	1.357	6.14	± 0.03		
		7	0.00	22.3	0.018	1.377	6.23	± 0.02		
		8	0.16	15.6	0.017	1.374	6.22	± 0.02		
		9	0.06	13.5	0.017	1.381	6.25	± 0.03	6.25 ± 0.02	
		fuse	0.00	28.4	0.017	1.388	6.28	± 0.01		
						Integrated age =	*6.21*	*± 0.01*		
Ro-3c	0.002520	1	19.15	0.8	0.050	1.638	7.41	± 0.43		
		2	4.67	1.7	0.020	1.336	6.05	± 0.22		**Tuff Ro-3 :**
		3	1.58	3.6	0.017	1.356	6.14	± 0.16		**6.20 ± 0.02**
		4	2.47	5.7	0.021	1.341	6.07	± 0.11	6.15 ± 0.02	
		5	0.68	10.0	0.019	1.363	6.17	± 0.07		
		fuse	0.42	78.2	0.017	1.361	6.16	± 0.01		
						Integrated age =	*6.16*	*± 0.02*		
Ro-3d	0.002520	1	1.76	0.1	0.147	2.636	11.92	± 4.77		
		2	0.00	0.5	0.053	1.557	7.04	± 0.68		
		3	0.00	0.6	0.057	1.422	6.44	± 0.58		
		4	3.68	2.6	0.034	1.336	6.05	± 0.13		
		5	2.67	4.0	0.025	1.351	6.11	± 0.09		
		6	1.06	15.5	0.019	1.370	6.20	± 0.03		
		7	0.81	16.7	0.018	1.365	6.18	± 0.03		
		8	0.30	8.8	0.019	1.376	6.23	± 0.04	6.21 ± 0.03	
		9	0.22	26.4	0.018	1.376	6.23	± 0.02		
		fuse	0.63	25.0	0.018	1.373	6.21	± 0.02		
						Integrated age =	*6.21*	*± 0.01*		
Ro-3	0.002520	fuse	0.24	-	0.017	1.360	6.16	± 0.02		
		fuse	0.58	-	0.017	1.369	6.20	± 0.01		
		fuse	0.10	-	0.016	1.364	6.18	± 0.01		
		fuse	0.12	-	0.016	1.367	6.19	± 0.01		
		fuse	0.11	-	0.017	1.371	6.21	± 0.01		
		fuse	0.12	-	0.016	1.386	6.27	± 0.01		
		fuse	0.03	-	0.018	1.369	6.20	± 0.01		
Ro-4a	0.002506	1	71.24	0.1	0.017	0.572	2.59	± 4.54		
		2	0.00	2.3	0.016	1.348	6.09	± 0.27		
		3	0.53	6.1	0.017	1.302	5.88	± 0.12		
		4	1.90	13.6	0.017	1.286	5.81	± 0.06		
		5	1.13	25.6	0.017	1.298	5.86	± 0.03	5.89 ± 0.04	
		6	2.14	8.9	0.017	1.287	5.81	± 0.09		
		7	0.00	11.5	0.017	1.319	5.96	± 0.05		
		fuse	0.31	31.8	0.017	1.317	5.95	± 0.02		
						Integrated age =	*5.89*	*± 0.02*		
Ro-4b	0.002506	1	4.70	3.0	0.017	1.319	5.96	± 0.18		
		2	0.00	3.2	0.016	1.295	5.85	± 0.18		
		3	0.43	3.9	0.017	1.298	5.86	± 0.19		
		4	3.80	4.4	0.018	1.245	5.62	± 0.13		
		5	2.43	25.6	0.017	1.270	5.74	± 0.03	5.77 ± 0.04	
		6	0.78	13.7	0.016	1.282	5.79	± 0.05		
		7	2.41	10.7	0.016	1.263	5.70	± 0.06		
		fuse	0.65	35.6	0.016	1.288	5.82	± 0.02		
						Integrated age =	*5.78*	*± 0.02*		
Ro-4c	0.002506	1	25.41	0.9	0.029	1.189	5.37	± 0.67		
		2	1.98	1.5	0.023	1.289	5.82	± 0.34		
		3	1.76	3.4	0.019	1.275	5.76	± 0.22		
		4	4.90	7.2	0.017	1.278	5.77	± 0.12		
		5	1.64	14.2	0.017	1.275	5.76	± 0.08		
		6	0.11	16.7	0.016	1.295	5.85	± 0.04		**Tuff Ro-4 :**
		7	0.00	13.7	0.016	1.298	5.86	± 0.05	5.84 ± 0.04	**5.87 ± 0.02**
		8	1.69	7.7	0.016	1.284	5.80	± 0.08		
		9	0.00	12.7	0.016	1.306	5.90	± 0.05		
		fuse	0.51	22.1	0.016	1.302	5.88	± 0.03		
						Integrated age =	*5.83*	*± 0.02*		
Ro-4d	0.002506	1	35.81	0.7	0.025	1.497	6.76	± 0.89		
		2	3.84	1.1	0.024	1.257	5.66	± 0.54		
		3	0.00	1.8	0.016	1.299	5.87	± 0.32		
		4	3.69	2.9	0.023	1.246	5.63	± 0.23		
		5	0.98	6.2	0.018	1.296	5.85	± 0.13		
		6	0.00	11.5	0.016	1.299	5.87	± 0.05		
		7	0.00	16.5	0.016	1.307	5.90	± 0.06	5.88 ± 0.04	
		8	0.00	9.4	0.015	1.301	5.87	± 0.08		
		9	0.01	41.7	0.016	1.303	5.88	± 0.02		
		fuse	0.35	8.2	0.015	1.301	5.87	± 0.08		
						Integrated age =	*5.88*	*± 0.02*		

Table 1 (Contd.)

Ro-4e	0.002506	1	40.61	0.2	0.103	1.836	8.29 ± 4.53		
		2	15.81	0.5	0.026	1.198	5.41 ± 2.62		
		3	2.14	0.9	0.039	1.305	5.90 ± 0.78		
		4	0.00	1.8	0.037	1.306	5.90 ± 0.51		
		5	7.48	2.7	0.028	1.212	5.48 ± 0.31		
		6	0.00	7.5	0.014	1.301	5.88 ± 0.14		
		7	0.49	19.4	0.016	1.290	5.83 ± 0.04		
		8	0.00	22.0	0.015	1.297	5.86 ± 0.05		
		9	0.47	15.1	0.015	1.290	5.83 ± 0.04	5.84 ± 0.04	
		10	2.24	5.5	0.015	1.273	5.75 ± 0.12		
		11	3.06	4.7	0.016	1.259	5.69 ± 0.13		
		fuse	0.00	19.8	0.015	1.306	5.90 ± 0.03		
						Integrated age =	*5.83 ± 0.03*		
Ro-4	0.002506	fuse	0.69	-	0.018	1.276	5.76 ± 0.03		
		fuse	0.33	-	0.016	1.303	5.88 ± 0.02		
		fuse	4.56	-	0.017	1.319	5.96 ± 0.02		
		fuse	7.28	-	0.016	1.291	5.83 ± 0.02		
		fuse	0.12	-	0.016	1.314	5.93 ± 0.03		
		fuse	0.00	-	0.016	1.293	5.84 ± 0.02		
		fuse	0.23	-	0.016	1.31	5.90 ± 0.02		
		fuse	0.00	-	0.016	1.32	5.94 ± 0.01		
		fuse	0.00	-	0.017	1.307	5.90 ± 0.01		
		fuse	0.66	-	0.017	1.294	5.84 ± 0.03		
		fuse	0.24	-	0.016	1.289	5.82 ± 0.01		
		fuse	0.19	-	0.017	1.302	5.88 ± 0.01		
Tiz-3a	0.002504	1	0.00	0.4	0.045	1.851	8.35 ± 1.96		
		2	0.00	0.5	0.020	1.405	6.34 ± 2.01		
		3	0.00	2.6	0.016	1.328	5.99 ± 0.35		
		4	0.00	12.2	0.017	1.309	5.91 ± 0.05		
		5	1.80	15.7	0.017	1.270	5.73 ± 0.05		
		6	0.00	29.8	0.017	1.299	5.86 ± 0.04		
		7	0.00	14.5	0.017	1.303	5.88 ± 0.05	5.85 ± 0.04	
		8	1.27	5.9	0.017	1.293	5.84 ± 0.13		
		fuse	0.06	18.6	0.017	1.305	5.89 ± 0.04		
						Integrated age =	*5.87 ± 0.02*		
Tiz-3b	0.002504	1	0.00	1.3	0.036	1.406	6.34 ± 0.71		
		2	0.00	1.8	0.017	1.313	5.92 ± 0.52		
		3	0.00	5.3	0.015	1.311	5.92 ± 0.18		
		4	1.91	9.2	0.017	1.281	5.78 ± 0.08		**Tuff Tiz-3 :**
		5	0.65	17.2	0.015	1.299	5.86 ± 0.05		**5.86 ± 0.03**
		6	0.88	19.8	0.016	1.295	5.84 ± 0.05	5.87 ± 0.04	
		7	0.00	9.1	0.015	1.309	5.91 ± 0.05		
		fuse	0.17	36.4	0.015	1.308	5.90 ± 0.02		
						Integrated age =	*5.88 ± 0.02*		
Tiz-3c	0.002504	1	100	0.1	-	-	- ± -		
		2	75.92	0.8	0.063	0.398	1.80 ± 1.73		
		3	78.85	0.7	0.078	0.279	1.26 ± 1.74		
		4	5.67	6.3	0.020	1.261	5.69 ± 0.28		
		5	3.61	7.2	0.019	1.273	5.75 ± 0.24		
		6	8.65	10.2	0.023	1.207	5.45 ± 0.17		
		7	2.27	18.2	0.020	1.278	5.77 ± 0.08		
		8	2.04	19.6	0.020	1.281	5.78 ± 0.09		
		9	1.45	12.6	0.018	1.293	5.84 ± 0.15	5.84 ± 0.1	
		10	0.00	6.9	0.013	1.319	5.95 ± 0.22		
		fuse	0.00	17.3	0.016	1.318	5.95 ± 0.10		
						Integrated age =	*5.87 ± 0.05*		
Car-2a	0.002516	1	10.37	0.6	0.021	1.452	6.58 ± 1.30		
		2	0.00	1.4	0.022	1.343	6.09 ± 0.69		
		3	0.00	5.2	0.018	1.318	5.97 ± 0.17		
		4	1.52	8.9	0.018	1.303	5.91 ± 0.07		
		5	0.18	24.2	0.017	1.317	5.97 ± 0.04		
		6	1.07	18.9	0.017	1.301	5.90 ± 0.04	5.95 ± 0.04	
		7	0.29	16.5	0.018	1.311	5.95 ± 0.05		
		fuse	0.08	24.5	0.017	1.317	5.97 ± 0.03		
						Integrated age =	*5.95 ± 0.02*		
Car-2b	0.002516	1	43.72	0.1	0.349	1.348	6.11 ± 3.51		
		2	0.92	0.4	0.011	1.361	6.17 ± 1.00		
		3	0.00	1.0	0.016	1.316	5.97 ± 0.38		**Sample Car-2 :**
		4	0.00	1.9	0.016	1.306	5.92 ± 0.19		**5.91 ± 0.02**
		5	0.00	5.9	0.016	1.303	5.91 ± 0.06		
		6	0.00	8.3	0.016	1.301	5.90 ± 0.05		
		7	0.02	19.8	0.016	1.300	5.89 ± 0.02		
		8	0.00	28.8	0.016	1.302	5.90 ± 0.02	5.90 ± 0.02	
		9	0.37	13.9	0.016	1.299	5.89 ± 0.03		
		fuse	0.25	19.9	0.015	1.306	5.92 ± 0.03		
						Integrated age =	*5.90 ± 0.01*		
Car-2c	0.002516	1	39.61	26.9	0.016	1.295	5.87 ± 0.07		
		2	0.42	27.0	0.016	1.287	5.84 ± 0.04	5.87 ± 0.04	
		fuse	0.79	46.2	0.015	1.298	5.88 ± 0.03		
						Integrated age =	*5.87 ± 0.02*		

% ^{39}Ar = fraction of ^{39}Ar released for each step; $^{40}Ar_{atm}$ = atmospheric ^{40}Ar; $^{40}Ar^*$ = radiogenic ^{40}Ar; Ar_{Ca} and Ar_K = Ar produced by Ca and K neutron interferences, respectively. The gas fractions corresponding to plateau ages are indicated by a dashed line at the right of the apparent ages. *Error bars* on apparent and integrated ages are given at the 1σ confidence level. Correction factors for interfering isotopes produced by neutrons in the McMaster reactor were measured in Nice, as $(^{39}Ar/^{37}Ar)Ca = 7.06\times10^{-4}$ (±4%), $(^{36}Ar/^{37}Ar)_{Ca} = 2.79\times10^{-4}$ (± 3%), and $(^{40}Ar/^{39}Ar)_K = 2.97\times10^{-2}$ (± 3%)

ages is 5.86 ± 0.02 Ma. The more variable low-temperature apparent ages (affected by larger error bars) relate to a contamination by alteration phases, as shown by both atmospheric contamination and variable $^{37}Ar_{Ca}/^{39}Ar_K$ ratios. Twelve total fusion analyses were also conducted on single crystals. The resulting age values scatter between 5.76 ± 0.06 and 5.96 ± 0.04 Ma. The lower age values may be caused by alteration whereas the slightly higher age values may originate from excess Ar or correspond to xenocrysts. The age

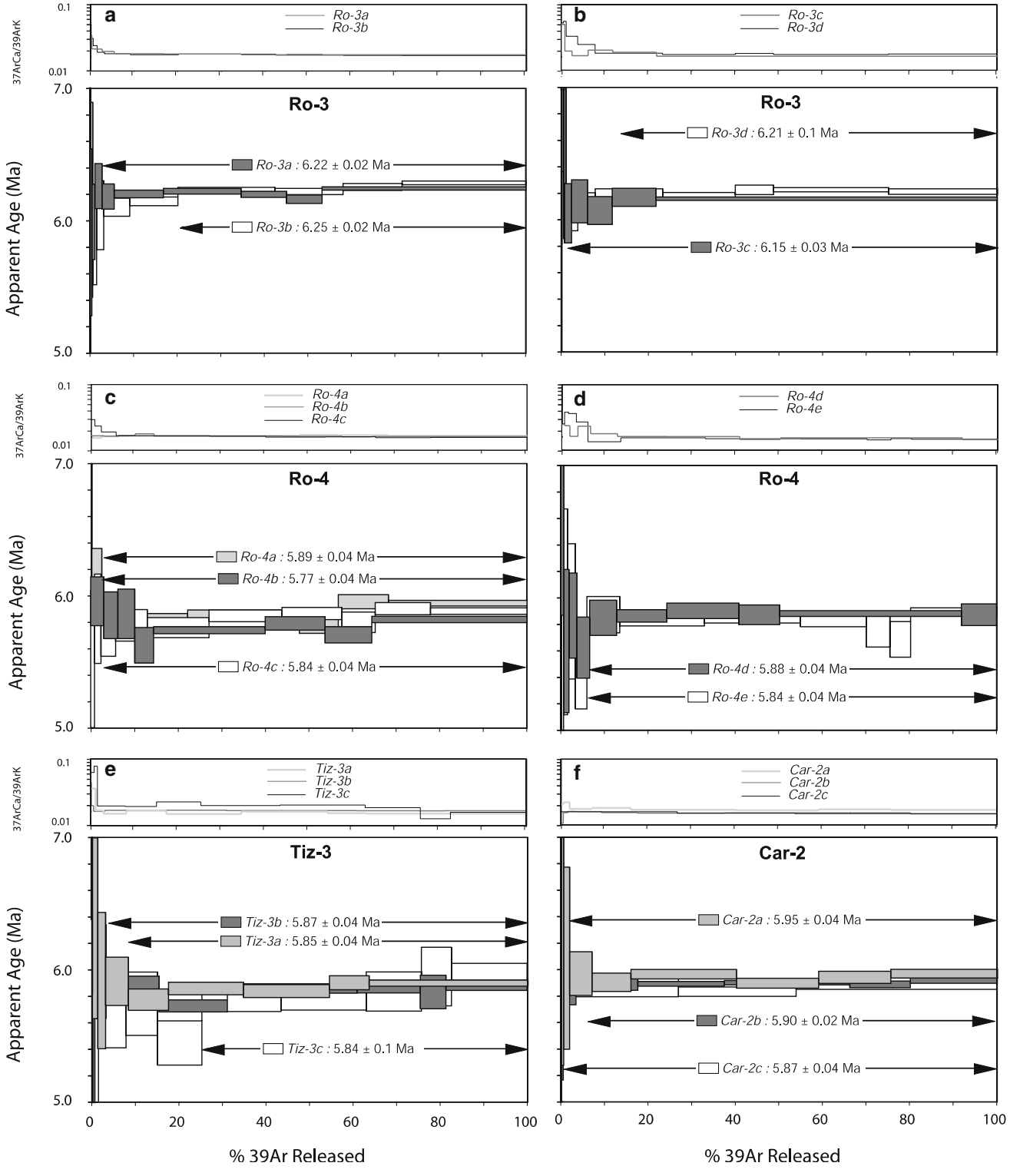

Fig. 3 $^{40}Ar/^{39}Ar$ ages and $^{37}Ar_{Ca}/^{39}Ar_K$ ratio spectra for the sanidine crystals from the studied tuffs. *Arrows* show the steps included in the plateau age calculations for each experiment (error at the 2σ level)

distribution of all data (plateau and single fusion ages) gives a peak at 5.87 Ma (Fig. 4). The weighted mean of concordant ages (four plateau ages and eight single fusion ages, plain symbols in Fig. 4) is 5.87 ± 0.02 Ma and corresponds to the accepted age. The weighted mean of all data yields exactly the same result. The inverse isochron plot for all data (not given) produces an age of 5.86 ± 0.03 Ma (MSWD = 2.3 and an initial $^{40}Ar/^{36}Ar$ ratio of 322 ± 15). The isochron plot of the concordant plateau fractions and fusion steps displays very clustered

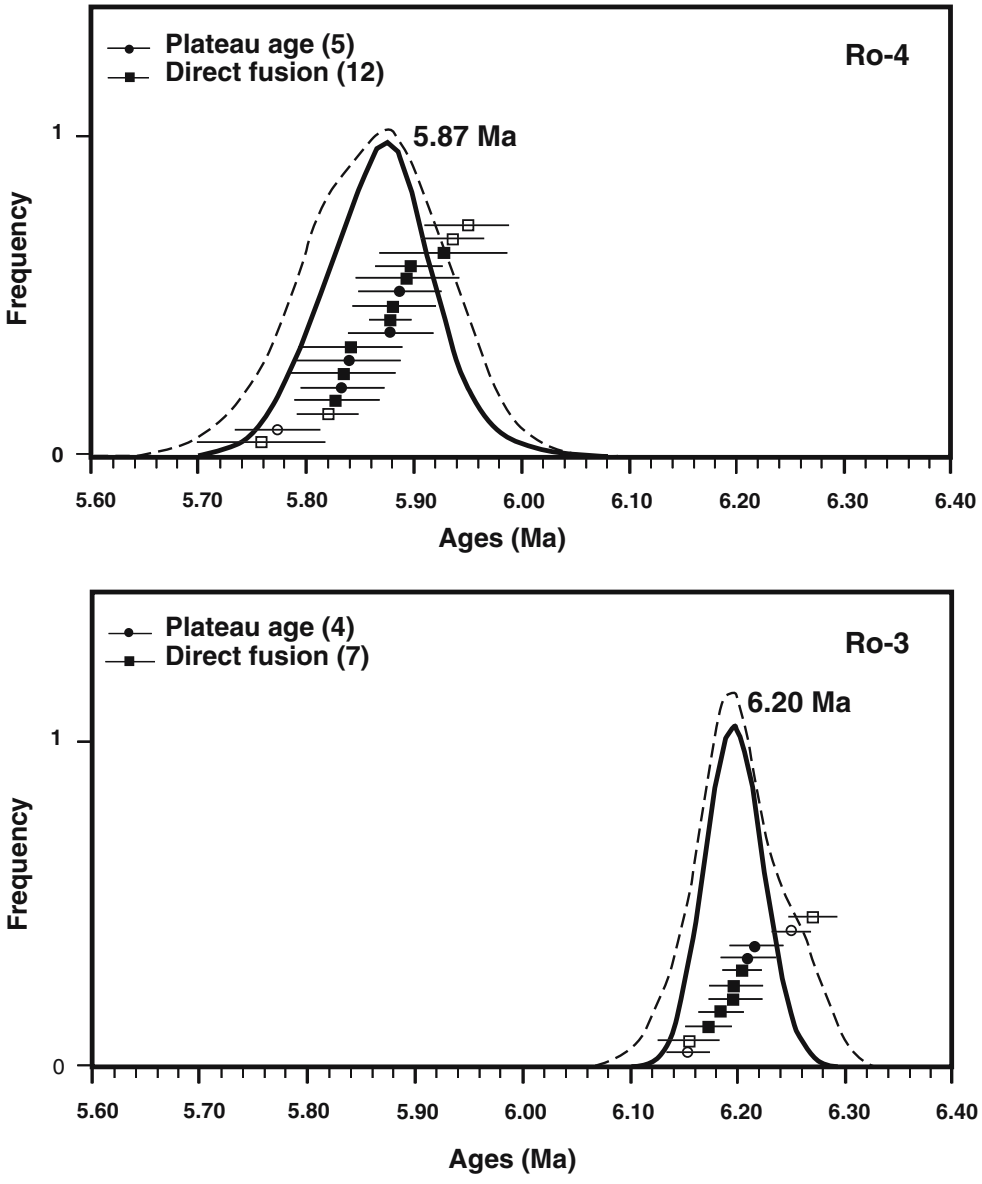

Fig. 4 Age distribution diagrams for single-crystal single fusion and step heating experiments. The *plain symbols* correspond to the data concordant at the 2σ level used to calculate weighted mean age in the text (= accepted age) whereas *open symbols* correspond to non-concordant data. The *dashed line* corresponds to the age distribution for the whole data set whereas the *plain line* corresponds to the age distribution for concordant data. The age for the data peak is shown as are individual data points and associated errors

data and an age of 5.88 ± 0.03 Ma (MSWD = 1.2 and an initial $^{40}Ar/^{36}Ar$ ratio of 271.6 ± 13.7).

Three single crystals from the Tiz-3 tuff (Fig. 2) yielded concordant plateau ages ranging from 5.84 ± 0.10 to 5.87 ± 0.04 Ma and correspond to at least 75% of the ^{39}Ar released (Fig. 3e). The weighted mean age is 5.86 ± 0.03 Ma. Because the atmospheric contamination is very low, no information could be obtained from isochron plots.

The three single crystals from the Car-2 tuff (Fig. 2) yielded concordant plateau ages ranging from 5.87 ± 0.04 to 5.95 ± 0.04 Ma corresponding to more than 96% of the ^{39}Ar released (Fig. 3f). The weighted mean age of 5.91 ± 0.02 Ma (= accepted age) is concordant with the Tiz-3 and Ro-4 weighted means (5.86 ± 0.03 and 5.87 ± 0.02 Ma, respectively) whereas they should have a younger age according to their relative stratigraphic positions. Therefore, the age of the Car-2 tuff is not stratigraphically consistent and may indicate a reworked origin for this deposit that may be sourced from the underlying "Pink Tuff" (Tiz-3 and Ro-4 samples).

In summary, these results allow us to define a timeline at 5.87 ± 0.02 Ma. Hence this can be used to precisely correlate the different TCC deposits (Fig. 2).

Discussion

Previous geochronological studies in the Melilla basin

For comparative purposes, previous data (Cunningham et al. 1994, 1997) have been recalculated relatively to an age of 28.02 Ma for the FCTs standard (Table 2) as recommended by Renne et al. (1998). For these comparisons, the precision of age measurements is the cru-

Table 2 Comparison between previously published $^{40}Ar/^{39}Ar$ data and this study

Tuff layer	Stratigraphic unit	Cunningham et al. (1997)		Kuiper (2003)	This study
		Published age	Re-calculated age using FCTs at 28.02 Ma		
V4a	TCC sub-cycle 2b	5.79 ± 0.04 Ma	5.85 ± 0.04 Ma		
Car-2	TCC sub-cycle b				5.91 ± 0.02 Ma
Tiz-3	TCC sub-cycle 2a				5.86 ± 0.03 Ma
V4	TCC sub-cycle 2a	5.82 ± 0.04 Ma	5.88 ± 0.04 Ma		
Ro-4 = V3	TCC sub-cycle 2a	5.95 ± 0.2 Ma	6.01 ± 0.2 Ma		5.87 ± 0.02 Ma
Ro-3 = Ifo-5	Pre-TCC			6.21 ± 0.02 Ma	6.20 ± 0.02 Ma

Errors are quoted at the 2σlevel. The age for Ro-3 = Ifo-5 in Kuiper (2003) was originally calculated using an age of 28.02 Ma for FCTs standard

cial parameter, although their accuracy is relative to the age of the FCT sanidine standard. Cunningham et al. (1994, 1997) dated five tuffs among which three occurred at three distinct stratigraphic levels within the TCC deposits (V3, V4, and V4a; Fig. 2 in Cunningham et al. 1997). We can place all three samples within the sub-cycle 2a of the TCC as defined herein. The V3 (= Ro-4) tuff, located a few metres above the *Halimeda* index-beds in the Rostrogordo section, yields a recalculated age of 6.01 ± 0.20 Ma (5.95 ± 0.20 Ma, 2σ, in Cunningham et al. 1994, 1997) and was proposed to fall within the upper part of the normal paleomagnetic sub-chron C3An.1n (Cunningham et al. 1994, 1997). From our results, we now consider a more precise age for V3 (= Ro-4) at 5.87 ± 0.02 Ma. The V4 tuff, located between the first two aggrading reefs from the TCC in the Ifo-unassene section, yields a recalculated age of 5.88 ± 0.04 Ma (5.82 ± 0.04 Ma, 2σ, in Cunningham et al. 1994, 1997) and was proposed by Cunningham et al. (1994, 1997) to fall within the sub-chron C3r. However, recent detailed sedimentological investigations proposed that there is only one volcanic tuff some metres above the base of the TCC within the northern platform (Cornée et al. 2002). Considering our more precise age for Ro-4 = V3 (5.87 ± 0.02 Ma), we observe that V3 and V4 (5.88 ± 0.04 Ma) have concordant ages. The similar ages for Ro-4 = V4 and V3 confirm the data of Cornée et al. (2002) who found only one major volcanic layer in the lowermost part of the TCC in the northern platform of Melilla. However, they disagree with the stratigraphic and paleomagnetic data presented in Cunningham et al. (1994). Cunningham et al. (1994) proposed that two tuffs are around 35 m apart. If true, that should yield an unrealistic vertical accumulation rate of 50 cm/kyr considering the refined age of Ro-4 (e.g. Cenozoic reefs: 3–28.6 cm/kyr; Miocene Great Barrier: 6.7–10 cm/kyr; Enos 1991). Thus, following our field observations, we propose a unique volcanic tuff which can be used as a time line at 5.87 ± 0.02 Ma. This allows us to define a new and precise correlation between basinal and coastal deposits. This result strongly suggests a reinterpretation of the available paleomagnetic data of Cunningham et al. (1994).

The V4a tuff, located immediately below the large oolitic deposits of the TCC in the Medouar area, yields a recalculated age of 5.85 ± 0.04 Ma (5.79 ± 0.04 Ma, 2σ, in Cunningham et al. 1997) and was proposed to fall within sub-chron C3r (Cunningham et al. 1997). Although the exact location of this tuff could not be determined, we can position it following the literature (Fig. 2 in Cunningham et al. 1997), exactly at the top of our TCC sub-cycle 2a. Then the age of the V4a sample is concordant with the age of Ro-4 tuff (5.87 ± 0.02 Ma; maximum age difference of 90 kyr when error bars are considered) although the V4a tuff is stratigraphically much more elevated than Ro-4. The V4a sample could have an epiclastic or re-worked origin rather than a pyroclastic one, similar to our Car-2 sample. Indeed, these two samples are both located within the upper part of sub-cycle 2a, in very shallow shoreface and high-energy environments.

The Ro-3 tuff has been re-dated at 6. 21 ± 0.02 Ma using only single grain total fusion techniques (sample no. Ifo-5 in Kuiper 2003). This age agrees very well with our value of 6.20 ± 0.02 Ma.

Correlations in the Melilla basin based on $^{40}Ar/^{39}Ar$ ages and sedimentology

From their similar age and mineralogy, the Ro-3 tuff (6.20 ± 0.02 Ma) and the aerial Bh-26 ignimbrite (6.23 ± 0.06 Ma: Roger et al. 2000), in the southwestern part of the Melilla basin (Bou Hamza area, Fig. 1), can now be correlated. The Bh-26 ignimbrite indicates emersion of the southwestern margin of the Melilla basin and marks the end of carbonate platform growth at that position.

The age of the base of the TCC within the Melilla basin was previously (Cornée et al. 2002) estimated to be at around 6.1 Ma using the available age for the V3 = Ro-4 tuff (Table 2; Cunningham et al. 1994, 1997). Now, we can re-evaluate this age using our more accurate age for the V3 = Ro-4 tuff (5.87 ± 0.02 Ma). Taking into account error bars, the age of the base of the TCC can be estimated at around 5.95–5.99 Ma. The age of the base of the *Halimeda* index-beds can also be estimated using vertical accumulation rates calculated for the marls/diatomite sequence (Münch et al. 2003). The calculated average vertical accumula-

tion rate of 8.3–8.6 cm/kyr yields an age at around 6.1 Ma for the base of *Halimeda* index-beds, which is in good accordance with the astronomical age, also established in the Melilla basin, of 6.07 Ma (Kuiper 2003). Therefore, the 68-m-thick reefal sequence, occurring between the base of *Halimeda*-rich talus and the base of V4 tuff, has an average vertical accumulation rate between 27.2 and 32.4 cm/kyr. These rates are close to the highest ones estimated for Cenozoic coral reefs (3–28.6 cm/kyr; Enos 1991). The base of the TCC (surface B; Fig. 2) in the Melilla basin thus cannot correspond to a hiatus of long duration considering both the age of tuffs surrounding the surface B and the very high vertical accumulation rates of the last fringing reefs.

Within the TCC sub-cycle 2a, we can now delineate a time line at 5.87 ± 0.02 Ma from the northern margin (Ifounassene and Rostrogordo sections) to the emerged foothill of the Gourougou volcano (Mallatcha and Tizza sections) through a passageway between the two margins of the basin (In Allah section) and the southern margin−continent transition (Medouar and Mallatcha sections; Fig. 2). The general facies distribution shows that the sub-cycle 2b TCC marine deposits (oolitic/stromatolitic and deltaic facies), mainly observable near the northeastern margin, are the lateral equivalent of continental-lagoonal deposits occurring in the vicinity of the Gourougou volcano (Mixed Carbonate Siliciclatic Complex in Cunningham et al. 1997). Rouchy et al. (2003) tentatively compared these continental deposits with the latest Messinian Lago-Mare facies and proposed they correspond to an early (~5.8 Ma) fresh water dilution of the Melilla basin, prior to the generalized and typical Lago-Mare episode at 5.52–5.33 Ma (Krijgsman et al. 2001). As the occurrence of continental deposits is related to the local paleogeography and as uppermost Messinian deposits (sub-cycle 2c at ~5.8 Ma) are still littoral oolitic/stromatolitic facies near the northern margin (Medouar and In Allah sections, Fig. 2), no early dilution of the Paleo-Mediterranean Sea can be evidenced within the Melilla basin. Our results show that the Lago-Mare deposits are completely lacking in the Melilla basin, whether non-deposited or eroded prior to the cycle 3 transgression. The general facies distribution shows that, during the TCC, the carbonate factory (coral reefs and then oolitic/stromatolitic shoals) was mainly located on the northern margin of the Melilla basin (Fig. 2). It also shows that the disruption of (1) the carbonate platform on the southern margin and (2) TCC deposition in almost the entire basin is correlative with two main tectono-magmatic episodes of Gourougou volcano that we can date at 6.2 and 5.8 Ma, respectively. These episodes may have contributed to the generalized emersion of the southern margin of the Melilla basin.

As the age of the cycle 3 lowermost deposits is not definitely established, the hiatus associated with the erosional surface at the top of the TCC appears to last approximately 450 kyr, between 5.77 ± 0.08 (age of the sub-aerial lava flow in the Medouar and Mallatcha sections; Cornée et al. 2002) and 5.33 Ma (M/P boundary; Lourens et al. 1996). This is a maximum duration for two reasons: (1) late Messinian deposits could have existed within the Melilla basin and have been later eroded, and (2) the marine re-flooding could be late Messinian or early Pliocene in age.

Implications for MSC

From a sedimentologic point of view, the TCC from the Melilla basin displays great similarities with the TCC in other Western Mediteranean marginal basins (Calvet et al. 1996; Esteban et al. 1996; Franseen et al. 1998). However, the former contains only two complete cycles, and locally a third one, whereas the latter generally show three to four cycles (Calvet et al. 1996; Franseen et al. 1998). This suggests that the preserved TCC in the Melilla basin could be incomplete, which agrees with an inferred generalized emersion of the basin at the top of TCC. However, our chronological data are in perfect accordance with the only chronological constraints available in the Cabo de Gata carbonate platform, in SE Spain (Franseen et al. 1998; Montgomery et al. 2001). There, the fringing coral reefs/TCC boundary falls in the lower portion of Chron C3r, which base was astronomically recalibrated at 6.04 ± 0.01 Ma (Krijgsman et al. 1999), and the whole TCC is restricted to this reversal Chron (Franseen et al. 1998; Montgomery et al. 2001). The last fringing reefs of Cabo de Gata are associated with *Halimeda*-rich talus as well as in the Melilla basin. This strongly suggests that these *Halimeda*-rich beds, slightly older than 5.95–5.99 Ma in the Melilla basin, represent time-equivalent event strata in the Western Mediterranean, as already suggested by Mankiewicz (1988) and Roger et al. (2000). Therefore, the base of the TCC, immediately overlying the *Halimeda* biosedimentary event, can also be considered synchronous over the entire Western Mediterranean.

This study demonstrates, for the first time, that the initiation of TCC deposition in the Melilla basin, estimated at 5.95–5.99 Ma, is synchronous with the onset of MSC, dated at 5.94–5.96 Ma throughout the Mediterranean Sea (Gautier et al. 1994; Krijgsman et al. 1999, 2001). As the unconformity separating the prograding reefs (cycle 1) from the TCC (cycle 2) within the Melilla basin is not a major sub-aerial surface and does not correspond to a significant hiatus (*sensu* Riding et al. 1999), the initiation of MSC does not correspond to a major sea-level drawdown. This is in agreement with many studies of Neogene basins in SE Spain (Sorbas: Roep et al. 1998; Conesa et al. 1999; Krijgsman et al. 1999—Nijar basin: Fortuin and Krijgsman 2002) and Western Algeria (Murdjadjo: Cornée et al. 1994). The preserved deposits of the TCC within the Melilla basin are thus time-equivalent with outcropping Lower

Evaporites of marginal basins. This result is in agreement with field observations made within Neogene basins in SE Spain (Santa Pola area: Calvet et al. 1996—Sorbas basin: Conesa et al. 1999—Nijar basin: Fortuin and Krijgsman 2002).

An apparent 450 kyr gap between cycles 2 and 3 within the Melilla basin is consistent with the timing of the MSC model of Clauzon et al. (1996). These authors proposed a drastic Mediterranean drawdown around 5.6 Ma, followed by a hiatus in marginal settings, between 5.6 and 5.3 Ma and then an early Pliocene reflooding. Considering that the uppermost TCC and the whole typical Lago-Mare sediments were not deposited and/or eroded in the Melilla area, their duration (around 200 kyr for Lago-Mare according to Krijgsman et al. 2001) has to be taken into account to estimate the time gap in the general scenario of the MSC. Moreover, the age of the first transgressive deposits over the erosional surface capping the TCC in the Melilla basin is not well defined and could still be late Messinian in age. Therefore the duration of the hiatus should be much less than 450 kyr. The apparent 450 kyr hiatus in the Melilla basin appears to be partly related to a tectono-magmatic uplift and not only to a sea-level lowering, as proposed by Duggen et al. (2003) and Warny et al. (2003).

Conclusion

This study gives an example of high precision $^{40}Ar/^{39}Ar$ ages applied to paleoclimatic and paleoenvironmental sequences. It describes the precise time frame of the sedimentary development of the Upper Messinian TCC, which is restricted to a single magnetic chron lasting less than 900 kyr. The main results are the following:

1. The transition of prograding or fringing coral reefs to TCC within the Melilla carbonate complex is now estimated at around 5.95–5.99 Ma, allowing us to correlate it with the onset of evaporite deposition within other marginal basins (Krijgsman et al. 1999, 2001), and therefore with the onset of the MSC (Gautier et al. 1994; Krijgsman et al. 1999).
2. No significant hiatus can be associated with the lower boundary of TCC within the Melilla basin. In the Western Mediterranean Sea, the TCC deposition in littoral areas is therefore lateral- or time-equivalent with the Lower Evaporites deposition within the marginal basins. Therefore, the oolite/microbialite deposition of the diverse TCC on the margins of the Western Paleo-Mediterranean Sea may be considered as a mostly synchronous biosedimentary event.
3. A precise time line was established within the TCC deposits at 5.87 ± 0.02 Ma, demonstrating a lateral transition between shallow-water normal marine and lagoonal–continental environments in relation with the paleogeography of the Melilla basin and not to an early dilution of the Paleo-Mediterranean Sea.
4. The TCC deposits in the Melilla basin appear to be incomplete, in relation with the tectono-magmatic uplift of the whole Alboran realm (Duggen et al. 2003; Warny et al. 2003). Therefore, the apparent hiatus associated with its upper unconformity, lasting between 5.77 and 5.32 Ma, may not be related to the Mediterranean drawdown only. Its duration could be shorter considering that the 450 kyr time gap evaluated in the Melilla basin is time-equivalent of the uppermost TCC and entire Lago-Mare deposition in other marginal basins.

Acknowledgments The authors wish to thank Dr. K.J. Cunningham and an anonymous reviewer for their revisions. We also thank the topic editor, Dr. K. Hammerschmidt, for his very constructive comments. This work is a contribution to the French INSU-CNRS programme ECLIPSE II "Vers une évaluation spatio-temporelle détaillée de l'impact de la Crise de Salinité Messinienne et de ses facteurs de contrôle". The authors thank Dr J. Reijmer for his help to improve the English wording of the text. Thanks to L. Marillier for thin sections, and R. Notonier and A. Tonetto for ESEM technical assistance. Géosciences Azur contribution no. 704.

References

Azdimousa A, Bourgois J (1993) Les communications entre l'Atlantique et la Méditerranée par le couloir sud-rifain du Tortonien à l'actuel: stratigraphie séquentielle des bassins néogènes de la région du cap des Trois Fourches (Rif oriental, Maroc). J Afr Earth Sci 17:233–240

Braga JC, Martín JM (1996) Geometries of reef advance in response to relative sea-level changes in a Messinian (uppermost Miocene) fringing reef (Cariatiz reef, Sorbas basin, SE Spain). Sediment Geol 107:61–81

Calvet F, Zamarreno I., Vallès D (1996) Late miocene reefs of the Alicante-Elche basin, Southeast Spain. In: Franseen EK, Esteban M, Ward WC, Rouchy JM (eds) Models for carbonate stratigraphy from miocene reef complexes of mediterranean regions. Soc Econ Paleontol Mineral Concepts in Sedimentol Paleontol Ser 5:177–190

Cas RAF, Wright JV (1988) Volcanic successions, modern and ancient. Unwin Hyman Ltd., pp487

Clauzon G, Suc JP, Gautier F, Berger A, Loutre MF (1996) Alternate interpretation of the Messinian salinity crisis: controversy resolved? Geology 24:363–366

Conesa G, Saint Martin JP, Cornée JJ, Muller J (1999) Nouvelles contraintes sur la crise de salinité messinienne par l'étude d'une plate-forme carbonatée marginale (bassin de Sorbas, Espagne). C R Acad Sci Paris 328:81–87

Cornée JJ, Saint Martin JP, Conesa G, Muller J (1994) Geometry, palaeoenvironments, and relative sea-level (accomodation space) changes in the Messinian Murdjadjo carbonate platform (Oran, Western Algeria) Consequences. Sediment Geol 89:143–158

Cornée JJ, Saint Martin JP, Conesa G, André JP, Muller J, Benmoussa A (1996) Anatomie de quelques plates-formes carbonatées progradantes messiniennes de Méditerranée. Bull Soc Géol Fr 167:495–507

Cornée JJ, Roger S, Münch PH, Saint-Martin JP, Féraud G, Conesa G, Pestrea S (2002) Messinian events: new constraints from sedimentological investigations and new $^{40}Ar/^{39}Ar$ ages in the Melilla-Nador basin (Morocco). Sediment Geol 151:127–147

Cornée JJ, Saint Martin JP, Conesa G, Münch PH, André JP, Saint Martin S, Roger S (2004) Correlations and sequence stratigraphic model for Messinian carbonate platforms of the western and central Mediterranean. Int J Earth Sci 93:621–633

Cunningham KJ, Collins LS (2002) Controls on facies and sequence stratigraphy of an upper Miocene carbonate ramp and platform, Melilla basin, NE Morocco. Sediment Geol 146:285–304

Cunningham KJ, Farr MR, Rakic-El Bied K (1994) Magnetostratigraphic dating of an upper Miocene shallow-marine and continental sedimentary succession in northeastern Morocco. Earth Planet Sci Lett 127:77–93

Cunningham KJ, Farr MR, Rakic-El Bied K, McKenna LW (1997) Eustatic implications of late Miocene depositional sequences in the Melilla Basin, northeastern Morocco. Sediment Geol 107:147–165

Duggen S, Hoernle K, Van den Bogaard P, Rüpke L, Morgan JP (2003) Deep roots of the Messinian salinity crisis. Nature 422:602–605

El Bakkali S, Gourgaud A, Bourdier JL, Bellon H, Gundogdu N (1998) Post-collision Neogene volcanism of the Eastern Rif (Morocco): magmatic evolution through time. Lithos 45:523–543

Enos P (1991) Sedimentary parameters for computer modeling. In: Franseen EK, Watney WL, Kendall CGStC, Ross W (eds) Sedimentary modelling: computer simulations and methods for improved parameter definition, Kansas. Geol Surv Bull 233:63–99

Esteban M (1979) Significance of the Upper Miocene coral reefs of the western Mediterranean. Palaeogeogr Palaeoclimatol Palaeoecol 29:169–188

Esteban M, Braga JG, Martin J, De Santisteban C (1996) Western mediterranean reef complexes. In: Franseen EK, Esteban M, Ward WC, Rouchy JM (eds) Models for carbonate stratigraphy from Miocene reef complexes of Mediterranean regions. Soc Econ Paleontol Mineral. Concepts in Sedimentol Paleontol Ser 5:55–72

Fortuin AR, Krijgsman W (2002) The Messinian of the Nijar Basin (SE Spain): sedimentation, depositional environments and paleogeographic evolution. Sediment Geol 3141:1–30

Fortuin AR, Krijgsman W, Hilgen FJ, Sierro FJ (2000) Late Miocene Mediterranean desiccation: topography and significance of the 'Salinity Crisis' erosion surface on-land in southeast Spain: comment. Sediment Geol 133:167–174

Franseen EK, Goldstein RH, Farr MR (1998) Quantitative controls on location and architecture of carbonate depositional sequences: upper Miocene, Cabo de Gata region; SE Spain. J Sediment Res 68(2):283–298

Garcia F, Conesa G, Münch PH, Cornée JJ, Saint Martin JP, André JP (2004) Evolution des environnements littoraux du bassin de Melilla-Nador (Nord-Est Maroc) au Messinien supérieur entre 6,0 et 5,77 Ma. Geobios 37:23–36

Gautier F, Clauzon G, Suc JP, Cravatte J, Violanti D (1994) Age et durée de la crise de salinité messinienne. C R Acad Sci Paris 318:1103–1109

Guillemin M, Houzay JP (1982) Le Néogène post-nappe et le Quaternaire du Rif nord-oriental (Maroc). Stratigraphie et tectonique des bassins de Melilla, du kert, de Boudinar et du piedmont des kebdena, Notes Mém Serv Géol Maroc 314:7–238

Hsü KJ, Montadert L, Bernoulli D, Cita MB, Erikson A, Garrison RE, Kidd RG, Mélières F, Müller C, Wright R (1977) History of the Messinian salinity crisis. Nature 267:399–403

Krijgsman W, Hilgen FJ, Raffi I, Sierro FJ, Wilson DS (1999) Chronology, causes and progression of the Messinian salinity crisis. Nature 852–855

Krijgsman W, Fortuin AR, Hilgen FJ, Sierro FJ (2001) Astrochronology for the Messinian Sorbas basin (SE Spain) and orbital (precessional) forcing for evaporite cyclicity. Sediment Geol 140:43–60

Kuiper K (2003) Direct intercalibration of radio-isotopic and astronomical ages in the Mediterranean Neogene. PhD Dissertation, Geologica Ultraiectina, vol 235, pp1–223

Lourens LJ, Hilgen FJ, Zachariasse WJ, Van Hoof AAM, Antonarakou A, Vergnaud-Grazzini C (1996) Evaluation of the pliocene to early pleistocene astronomical time scale. Paleoceanography 11:391–413

Mankiewicz C (1988) Occurrence and paleoecologic significance of Halimeda in late Miocene reefs, southeastern Spain. Coral Reefs 6:271–279

Martín JM, Braga JC (1994) Messinian events in the Sorbas Basin in southeastern Spain and their implications in the recent history of the Mediterranean. Sediment Geol 90:257–268

Montgomery P, Farr MR, Franseen EK, Goldstein RH (2001) Constraining controls on carbonate sequences with high-resolution chronostratigraphy: upper Miocene, Cabo de Gata region, SE Spain. Paleogeogr Paleoclimatol Paleoecol 176:11–45

Münch PH, Roger S, Cornée JJ, Saint-Martin JP, Féraud G, Ben Moussa A (2001) Restriction des communications entre l'Atlantique et la Méditerranée au Messinien : apport de la téphrochronologie dans la plate-forme carbonatée et le bassin de Melilla-Nador (Rif nord-oriental, Maroc). C R Acad Sci Paris Sciences de la Terre et des planètes/Earth Planet Sci 332:569–576

Renne PR, Swisher CC, Deino AL, Karner DB, Owens T, De Paolo DJ (1998) Intercalibration of standards. Absolute ages and uncertainties in $^{40}Ar/^{39}Ar$ dating. Chem Geol (Isot Geosci Sect) 145:117–152

Renne PR, Swisher CC, Deino AL, Karner DB, Owens T, De Paolo DJ (1998) Intercalibration of standards. Absolute ages and uncertainties in $^{40}Ar/^{39}Ar$ dating. Chem Geol (Isot Geosci Sect) 145:117–152

Riding R, Braga JC, Martín JM (1999) Late Miocene Mediterranean dessication: topography and significance of the "Salinity Crisis" erosion surface on-land in southeast Spain. Sediment Geol 123:1–7

Riding R, Braga JC, Martin JM, Sanchez-Almazo IM (1998) Mediterranean Messinian salinity crisis: constraints from a coeval marginal basin, Sorbas, southeastern Spain. Mari Geol 146:1–20

Roep TB, Dabrio CJ, Fortuin AR, Polo MD (1998) Late highstands patterns of shifting and stepping coastal barriers and washover-fans (late Messinian, Sorbas Basin, SE Spain). Sediment Geol 116:27–56

Roger S, Münch PH, Cornée JJ, Saint Martin JP, Féraud G, Conesa G, Pestrea S, Benmoussa A (2000) $^{40}Ar/^{39}Ar$ dating of the pre-evaporitic Messinian marine sequences of the Melilla basin (Morocco): a proposal for some bio-sedimentary events as isochrons around the Alboran Sea. Earth Planet Sci Lett 179:101–113

Rouchy JM, Pierre C, Et-Touhami M, Kerzazi K, Caruso A, Blanc-Valleron MM (2003) Late Messinian to early pliocene paleoenvironmental changes in the Melilla Basin (NE Morocco) and their relation to Mediterranean evolution. Sediment Geol 163:1–27

Rouchy JM, Saint Martin JP (1992) Late Miocene events in the Mediterranean as recorded by carbonate-evaporite relations. Geology 20:629–632

Saint Martin JP, Cornée JJ (1996) The Messinian Melilla reef complex, Northeastern Rif, Morocco. In: Franseen EK, Esteban M, Ward WC, Rouchy JM (eds) Models for carbonate stratigraphy from Miocene reef complexes of Mediterranean regions. Soc Econ Paleontol Mineral. Concepts Sedimentol Paleontol Ser 5:227–237

Saint Martin JP, Cornée JJ, Muller J, Camoin G, André JP, Rouchy JM, Benmoussa A (1991) Contrôles globaux et locaux dans l'édification d'une plate-forme carbonatée messinienne (bassin de Melilla, Maroc): apport de la stratigraphie séquentielle et de l'analyse tectonique. C R Acad Sci Paris 315:1573–1579

Warny SA, Bart PJ, Suc J-P (2003) Timing and progression of climatic, tectonic and glacioeustatic influences on the Messinian Salinity Crisis. Palaeogeogr Palaeoclimatol Palaeoecol 202:59–66